View metadata, citation and similar papers at core.ac.uk
brought to you by CORE
provided by Archivio istituzionale della ricerca - Università di Brescia

Optics Letters

Spatiotemporal characterization of supercontinuum extending from the visible to the mid-infrared in a multimode graded-index optical fiber

K. Krupa,[1,2] C. Louot,[1] V. Couderc,[1] M. Fabert,[1] R. Guenard,[1] B. M. Shalaby,[1,3] A. Tonello,[1,*] D. Pagnoux,[1] P. Leproux,[1] A. Bendahmane,[2] R. Dupiol,[2] G. Millot,[2] and S. Wabnitz[4]

[1]Université de Limoges, XLIM, UMR CNRS 7252, 123 Avenue A. Thomas, 87060 Limoges, France
[2]Université de Bourgogne Franche-Comté, ICB UMR CNRS 6303, 9 Avenue A. Savary 21078 Dijon, France
[3]Physics Department, Faculty of Science, Tanta University, 31527 Tanta, Egypt
[4]Dipartimento di Ingegneria dell'Informazione and INO-CNR, Università di Brescia, via Branze 38, 25123 Brescia, Italy
*Corresponding author: alessandro.tonello@unilim.fr

Received 4 November 2016; accepted 13 November 2016; posted 21 November 2016 (Doc. ID 279740); published 15 December 2016

We experimentally demonstrate that pumping a graded-index multimode fiber with sub-ns pulses from a microchip Nd:YAG laser leads to spectrally flat supercontinuum generation with a uniform bell-shaped spatial beam profile extending from the visible to the mid-infrared at 2500 nm. We study the development of the supercontinuum along the multimode fiber by the cut-back method, which permits us to analyze the competition between the Kerr-induced geometric parametric instability and stimulated Raman scattering. We also performed a spectrally resolved temporal analysis of the supercontinuum emission. © 2016 Optical Society of America

OCIS codes: (060.4370) Nonlinear optics, fibers; (320.6629) Supercontinuum generation; (190.4410) Nonlinear optics, parametric processes.

https://doi.org/10.1364/OL.41.005785

The strong modal confinement and the versatile dispersion engineering of single-mode fibers (SMFs) have permitted to demonstrate efficient and spatially coherent supercontinuum (SC) sources spanning from the ultra-violet to the mid-infrared (MIR) [1]. However, the small mode area of SMFs limits the accepted energy to relatively low values (less than 20 μJ for sub-ns pulses). For this reason, SC sources based on SMFs cannot be used for applications where high pulse energies are required. Although multimode fibers (MMFs), such as graded-index (GRIN) fibers, permit the propagation of high energy pulses, these are subject to mode beating and mixing, owing to the difference of modal propagation constants and linear mode coupling. Modal interference brings a speckled intensity pattern at the MMF output, which prevents the use of MMFs whenever the preservation of spatial beam quality is required [2].

Recent experiments by Krupa *et al.* [3] led to the unexpected discovery that Kerr nonlinearity of glass fibers above a certain threshold pulse power may lead to the generation of a self-sustained bell-shaped nonlinear beam in a highly multimode GRIN fiber. This means that linear mode mixing can be effectively washed out by means of the Kerr effect, so that a cleaned multimode light beam remains effectively self-preserved. Kerr self-cleaning (KSC) stems from nonlinear coupling among the fundamental mode and higher-order modes [3,4]. KSC occurs at power levels at least one order of magnitude lower than the critical power of catastrophic light self-focusing in a GRIN MMF [5]. Because it is a conservative process, KSC is fundamentally different from the well-known Raman beam cleanup that is observed at the Stokes wavelength [6]. In addition, KSC occurs before a substantial pump spectral broadening has occurred [3]. For powers above the KSC threshold, nonlinear spectral broadening in MMFs results from a complex interplay between the spatial and temporal degrees of freedom [7–9]. Because of the self-imaging of the multimode beams in a GRIN MMF, the Kerr effect leads to a long-period intensity grating which induces mode conversion [4] and quasi-phase-matched (QPM) four-wave mixing (FWM) [10]. For temporal multimode femtosecond solitons in the anomalous dispersion regime [11], the nonlinear index grating produces an effective periodic nonlinearity which, in turn, induces a series of dispersive wave sidebands [12,13]. On the other hand, for a quasi-CW pump pulse propagating in the normal dispersion regime (in order to avoid the modulation instability induced breakup into an ultrashort soliton pulse train) the nonlinear index grating leads to a series of intense QPM-FWM (or geometric parametric instability [GPI]) sidebands in the visible and near-infrared (NIR) [7]. Quite remarkably, experiments of [7] revealed that the Kerr self-cleaning of the pump beam is frequency transferred across the entire spectrum of the GPI sidebands. Finally, for higher powers and fiber lengths, the GPI sidebands merge into a broadband SC

as a result of the interplay of the Kerr effect and Raman scattering, and both effects cooperate with each other in reinforcing the wideband spatial beam cleaning [8,9,14,15]. In particular, the dependence of SC generation on a GRIN MMF as a function of pump power was experimentally studied in [8,15]. In this Letter, we focus our attention instead on the study of the role of fiber length in determining the competition among the different mechanisms responsible for SC growth in GRIN MMFs and their consequences on the spectral shape. SC generation is accompanied by broadband beam cleaning; therefore, we simultaneously analyze spatial and temporal properties of the SC process. By cut-back measurements, we could identify the respective length scales for the development of visible and NIR spectral components. By numerical simulations, we are able to reproduce the basic features of broadband spatial beam cleaning along the fiber. In addition, we unveil a new mechanism of spectral flattening that occurs whenever the fiber length is properly optimized to an intermediate length: short fibers exhibit sharp discrete GPI sidebands, whereas long fibers result in broad SC spectra, but with large spectral ripples. Finally, by means of spectrally resolved temporal measurements, we could determine, by direct detection, the temporal envelopes associated with the GPI sidebands, the depleted pump, and the Stokes light at NIR wavelengths, respectively.

In our experiments, we used as a pump source an amplified Nd:YAG microchip laser, delivering 900 ps pulses at 1064 nm with a 30 kHz repetition rate. The linearly polarized Gaussian pump pulses were launched into the GRIN MMF (core diameter 52 μm, NA = 0.2) by using a lens with focal length of 50 mm and a three-axis translating stage. At the input face of the fiber, the beam had a FWHMI diameter of 40 μm, which is close to the fiber core diameter. We used an optical spectrum analyzer (OSA) covering the spectral range from 350 to 1750 nm, as well as a spectrometer covering the range from 850 to 2500 nm. The output beam profile was imaged on a CCD camera through a microlens with 8 mm focal length.

Figure 1 provides the experimental characterization of the optical spectrum at the output of a 12 m long GRIN MMF, as a function of the pump peak power. (The spectral levels in a decibel scale are referred to as the values at 1118 nm.) As can be seen, a visible SC develops until right below 500 nm whenever the pump peak power grows larger than 25 kW. In terms of spectral flatness, as the peak power reaches 35 kW, the SC amplitude remains relatively uniform until about 700 nm, beyond which it rapidly drops. On the other hand, spectral broadening on the infrared (IR) side of the pump continuously grows with pump power: above 25 kW of peak power, the SC extends beyond 1750 nm with remarkable spectral flatness (see the inset of Fig. 1). For understanding the dynamics of SC generation in a GRIN MMF under the combined action of Kerr effect and Raman scattering, it is crucial to study the growth of SC along the fiber length.

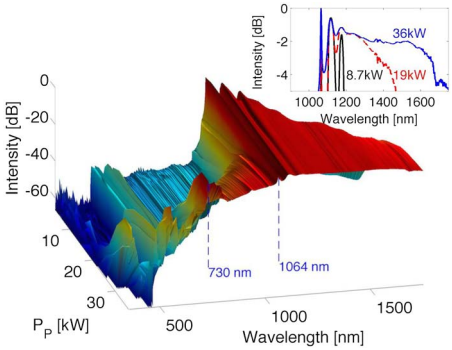

Fig. 1. Experimental SC spectra as a function of the pump pulse peak power P_p, for a fixed length of 12 m GRIN MMF. The inset shows that the spectral ripple at 1142 nm is reduced by 1.1 dB when increasing the power.

Figure 2 displays the results of cut-back experiments that describe the development of SC along the MMF for a fixed input average power of 1.4 W (51.8 kW input peak power). As can be seen, GPI and Raman provide the major contributions to the spectral broadening, but their effects manifest with different length scales. In the very first meter of propagation, GPI generates the first-order anti-Stokes sideband at about 730 nm, which carries around 12% of the total input power [7,10]. After 1.5 m of propagation, the Raman effect comes into play, causing a gradual spectral extension toward the infrared side of the spectrum: the resulting pump depletion in turn inhibits the GPI frequency conversion. For fiber lengths up to about 12 m, and for peak powers above 35 kW, the Raman-induced SC spectrum assumes an unusual flat shape in the IR. (See the inset that compares the lengths of 2, 12, and 30 m.) In parallel, after the first 3 m, the sideband at 730 nm, which is no longer fed, undergoes Raman and cross-phase modulation spectral broadening so that the gap between 730 and 1000 nm is gradually filled. For fiber segments longer than 20 m, the spectral broadening exhibits significant spectral ripples: the first three Raman Stokes sidebands between 1100 and 1350 nm can be easily identified (inset of Fig. 2).

More details about the longitudinal development of SC can be extracted from Fig. 3, where we compare the spatial evolution along the GRIN MMF of the power of selected spectral components from the spectra of Fig. 2. Figure 3 clearly shows that the components of the NIR spectrum between the Raman peaks (components at 1106 and at 1142 nm) reach their maximum values after about 2 m and have later on a gradual drop, consequently revealing the Raman sidebands. On the other hand, the SC components at 1550 and at 1650 nm only start to appear between 5 and 10 m, and reach their stationary power levels at above 15 m of MMF. Figure 3 also reveals that the first anti-Stokes GPI sideband at 730 nm initially overshoots to its

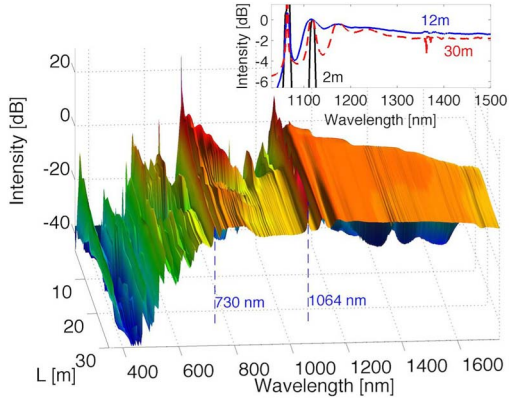

Fig. 2. Experimental results of the cut-back technique. (The input average power in the fiber 1.4 W drops to 670 mW after 30 m of fiber.) Inset: a fiber length $L = 12$ m reduces by 2.5 dB the spectral ripple at 1142 nm with respect to $L = 30$ m.

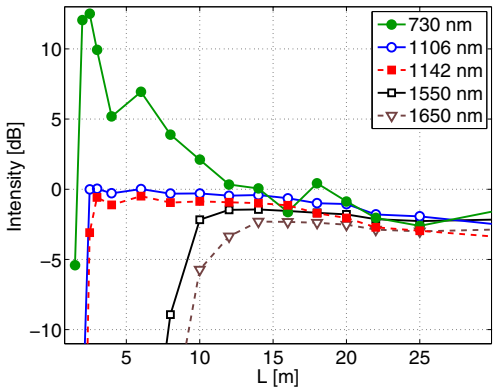

Fig. 3. Longitudinal evolution of the spectral intensity at selected spectral components from Fig. 2.

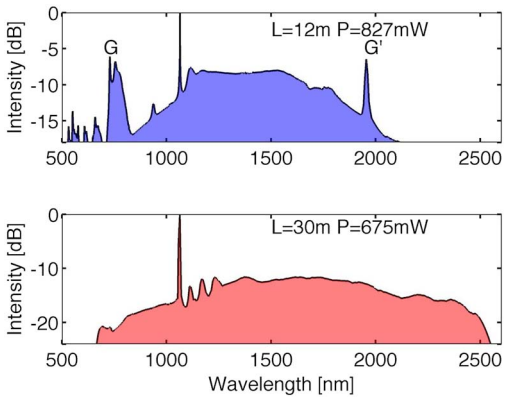

Fig. 5. Comparison of SC intensity profiles with 12 (top) and 30 m (bottom) of GRIN MMF.

peak power value within the first meter of fiber and, subsequently, relaxes down to the same steady-state power level (situated about 15 dB below the peak value) as all other components after 15 m of fiber length.

We performed extensive numerical simulations to model the observed SC generation dynamics and for understanding the relative balance of the Kerr and Raman scattering mechanisms as a function of the MMF length. We have solved the nonlinear Schrödinger equation with two transverse dimensions and one temporal dimension, including a truncated parabolic profile for describing the GRIN MMF refractive index, with both Kerr nonlinearity and stimulated Raman scattering [3]. In order to reduce the computational load, in our simulations, we considered relatively short (less than 1.4 m) fiber lengths by correspondingly increasing the beam intensity to 10 GW/cm^2; we also considered a pump pulse duration of 9 ps. Although this procedure is expected to provide only a qualitative correspondence with the experimental results, the numerical results of Fig. 4 reproduce fairly well the occurrence of sharp spectral peaks in the visible domain, as well as the development of a spectrally flat SC across the entire NIR along the course of propagation. The frames of Fig. 4 compare spatial transverse profiles

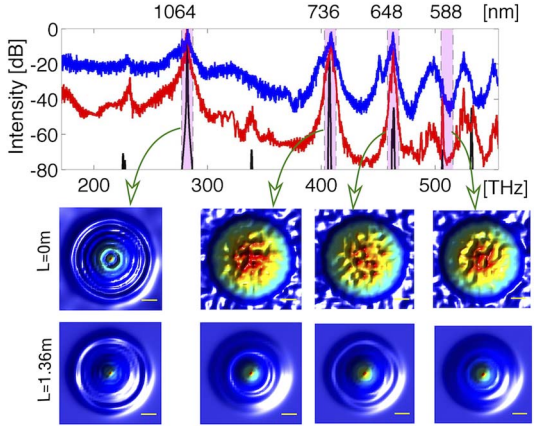

Fig. 4. Numerical simulation of SC generation in GRIN MMF. The upper panel demonstrates spectra at 0.16 (black), 0.42 (red), and 1.36 m (blue). The frames on the lower panel demonstrate the spatial profiles for the selected wavelength regions. Yellow segment length: 10 μm.

corresponding to selected spectral components at the beginning of the propagation and at the end of the fiber. The spectrum outside the pump is initiated by noise; at the end of the propagation, all beams exhibit a well-defined bell shape.

As shown in Fig. 5, where we combined the output of the OSA and of the spectrometer, we observed that, as the MMF length increases up to 30 m, SC generation can be extended into the MIR (i.e., up to 2500 nm). The result of Fig. 5 is remarkable, when considering the large linear absorption of the MMF in the MIR. The comparison of the SC intensity profiles obtained for 12 and 30 m reported in Fig. 5 clearly shows that the SC bandwidth also critically depends on the MMF length. Moreover, Fig. 5 reveals that the isolated GPI sidebands in the visible domain are better discernible for MMF lengths of about 10 m (or shorter, as discussed with reference to Fig. 3). On the other hand, spectral broadening is dominated by Raman scattering for MMF lengths above a few tens of meters [16].

Next we carried out a study of the wavelength dependence of the transverse beam profile emerging from the GRIN MMF. The plots of Fig. 6 show the far field at the output of the MMF analyzed by using a series of bandpass filters (10 nm bandwidth) with different center wavelengths. We observed that the spatial coherence acquired by the pump beam because of the Kerr self-cleaning effect [3] is effectively transferred

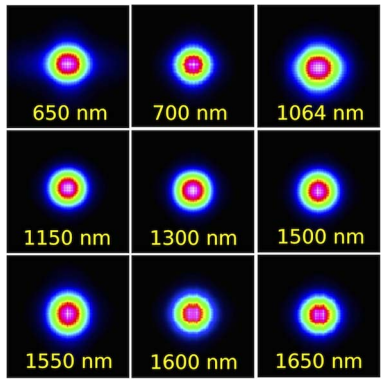

Fig. 6. Far field at the fiber output for $L = 30$ m, using different bandpass filters (10 nm bandwidth) and for 1.4 W input average power.

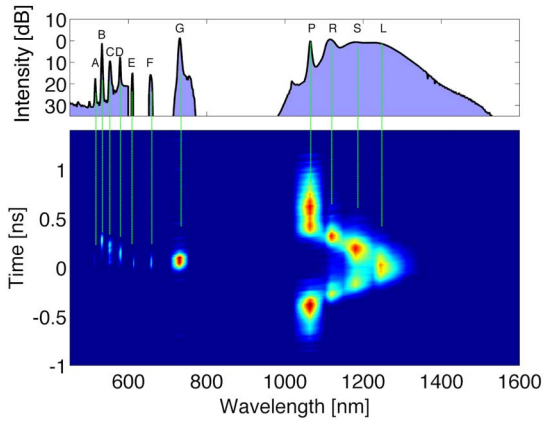

Fig. 7. Spectrum (upper panel) and spectro-temporal characterization (lower panel) of SC at the output of a 6 m long GRIN MMF. The letters indicate the following wavelengths: 515 nm (A), 532 nm (B), 552 nm (C), 578 nm (D), 610 nm (E), 656 nm (F), 730 nm (G), 1064 nm (P) 1116 nm (R), 1180 nm (L), and 1250 nm (S).

across the entire spectrum of the SC. Figure 6 shows that for all wavelengths a bell-shaped spatial profile is observed at the output of a GRIN MMF of length $L = 30$ m. As we have discussed with reference to Fig. 5, for this length of fiber, the main mechanism for generating the NIR side of the SC is the Raman effect, which also privileges bell-shaped beams. However similar results for near and far fields (not shown here) were also observed in the visible domain, as well as at the pump wavelength for fiber lengths shorter than 8 m, which is well before the Raman scattering threshold [7].

For potential applications of MMF SC sources, such as in multiplex CARS spectroscopy [17], it is important to consider the possibility of achieving simultaneous interactions among multiple wavelengths on a sample. To clarify the spectro-temporal structure of the generated SC radiation, we experimentally analyzed the variation of the temporal envelope across different wavelengths, as shown in Fig. 7. This was achieved by dispersing the fiber output light with a grating, which permitted us to analyze the temporal envelope with two different 12 GHz photodiodes (in order to cover both the visible and the NIR portions of the SC) and a 20 GHz oscilloscope. With our detection system we could not resolve temporal features below 83 ps. In Fig. 7 the electric signals have been rescaled in proportion to the corresponding local optical spectral power. Nevertheless, as shown in Fig. 7, our spectrogram revealed the presence of a deep temporal modulation within the flat portion of the NIR SC spectrum. In fact, Fig. 7 shows that the larger Raman frequency shift comes from the highest input peak power which, in turn, leads to the strongest pump pulse depletion at the MMF output. As a consequence, the different power values of the temporal profile of the input pump pulse are transposed into different wavelength shifts. A similar feature of frequency coding in time has been recently characterized in SMFs in [18]. The relatively short (6 m) MMF length could also permit us to clearly observe in Fig. 7 the temporal envelopes of the separate GPI sidebands (G indicates the first GPI sideband; see [7] for details). As can be seen, the GPI sideband durations are much shorter than the input pump pulse. The sideband G at 730 nm, whose envelope of 130 ps is seven times shorter than the pump, can be directly revealed.

In summary, we have shown that multimode GRIN fibers provide a new, intriguing, low-cost, and high-pulse-energy platform for SC generation ranging from the visible until the MIR. We demonstrated that pumping a GRIN MMF with a sub-nanosecond microchip laser in the normal dispersion regime permits to maintain the spatial beam quality of the SC, thanks to the cooperative action of Kerr self-cleaning and Raman beam cleaning effects. We performed an experimental characterization of the growth rate of parametric and Raman components, and we described the time-frequency structure of the generated supercontinuum.

Funding. Bpifrance OSEO; Horiba Medical Dat@diag.

Acknowledgment. The authors thank A. Barthélémy for insightful comments and helpful suggestions.

REFERENCES

1. J. M. Dudley, G. Genty, and S. Coen, Rev. Mod. Phys. **78**, 1135 (2006).
2. A. Picozzi, G. Millot, and S. Wabnitz, Nat. Photonics **9**, 289 (2015).
3. K. Krupa, A. Tonello, B. M. Shalaby, M. Fabert, A. Barthélémy, G. Millot, S. Wabnitz, and V. Couderc, "Spatial beam self-cleaning in multimode," arXiv:1603.02972 (2016).
4. M. Schnack, T. Hellwig, M. Brinkmann, and C. Fallnich, Opt. Lett. **40**, 4675 (2015).
5. J. Manassah, P. Baldeck, and R. Alfano, Opt. Lett. **13**, 589 (1988).
6. N. B. Terry, T. G. Alley, and T. H. Russell, Opt. Express **15**, 17509 (2007).
7. K. Krupa, A. Tonello, A. Barthélémy, V. Couderc, B. M. Shalaby, A. Bendahmane, G. Millot, and S. Wabnitz, Phys. Rev. Lett. **116**, 183901 (2016).
8. G. López-Galmiche, Z. S. Eznaveh, M. A. Eftekhar, J. E. Antonio-Lopez, F. W. Wise, D. N. Christodoulides, and R. Amezcua-Correa, in *Conference on Lasers and Electro-Optics* (Optical Society of America, 2016), paper STh4O.6.
9. S. Wabnitz, K. Krupa, A. Tonello, A. Bendahmane, R. Dupiol, B. Shalaby, M. Fabert, C. Louot, R. Guenard, A. Barthelemy, G. Millot, and V. Couderc, in *Latin America Optics and Photonics Conference* (Optical Society of America, 2016), paper LTh2A.2.
10. S. Longhi, Opt. Lett. **28**, 2363 (2003).
11. W. H. Renninger and F. W. Wise, Nat. Commun. **4**, 1719 (2013).
12. L. G. Wright, D. N. Christodoulides, and F. Wise, Nat. Photonics **9**, 306 (2015).
13. L. G. Wright, S. Wabnitz, D. N. Christodoulides, and F. Wise, Phys. Rev. Lett. **115**, 033838 (2015).
14. L. G. Wright, Z. Liu, D. A. Nolan, M.-J. Li, D. N. Christodoulides, and F. W. Wise, Nat. Photonics **10**, 771 (2016).
15. G. Lopez-Galmiche, Z. S. Eznaveh, M. A. Eftekhar, J. A. Lopez, L. G. Wright, F. Wise, D. Chirstodoulides, and R. A. Correa, Opt. Lett. **41**, 2553 (2016).
16. H. Pourbeyram, G. P. Agrawal, and A. Mafi, Appl. Phys. Lett. **102**, 201107 (2013).
17. K. Hiramatsu, M. Okuno, H. Kano, P. Leproux, V. Couderc, and H. Hamaguchi, Phys. Rev. Lett. **109**, 083901 (2012).
18. B. M. Shalaby, C. Louot, E. Capitaine, K. Krupa, A. Labruyère, A. Tonello, D. Pagnoux, P. Leproux, and V. Couderc, Opt. Lett. **41**, 5007 (2016).

94.37.183.78 {ts '2017-01-07 04:03:15'}